Functional interplay between protein domains in a supramodular structure involving the postsynaptic density protein PSD-95

Received for publication, September 16, 2019, and in revised form, December 12, 2019 Published, Papers in Press, December 12, 2019, DOI 10.1074/jbc.RA119.011050

Louise Laursen[‡], **Elin Karlsson**[‡], **Stefano Gianni**[§1], **and Per Jemth**[‡2]

From the [‡]*Department of Medical Biochemistry and Microbiology, Uppsala University, BMC Box 582, 75123 Uppsala, Sweden and the* [§]*Istituto Pasteur-Fondazione Cenci Bolognetti and Istituto di Biologia e Patologia Molecolari del CNR, Dipartimento di Scienze Biochimiche "A. Rossi Fanelli," Sapienza Università di Roma, 00185 Rome, Italy*

Edited by F. Peter Guengerich

Cell scaffolding and signaling are governed by protein–protein interactions. Although a particular interaction is often defined by two specific domains binding to each other, this interaction often occurs in the context of other domains in multidomain proteins. How such adjacent domains form supertertiary structures and modulate protein–protein interactions has only recently been addressed and is incompletely understood. The postsynaptic density protein PSD-95 contains a three-domain supramodule, denoted PSG, which consists of PDZ, Src homology 3 (SH3), and guanylate kinase-like domains. The PDZ domain binds to the C terminus of its proposed natural ligand, CXXC repeat– containing interactor of PDZ3 domain (CRIPT), and results from previous experiments using only the isolated PDZ domain are consistent with the simplest scenario for a protein–protein interaction; namely, a two-state mechanism. Here we analyzed the binding kinetics of the PSG supramodule with CRIPT. We show that PSG binds CRIPT via a more complex mechanism involving two conformational states interconverting on the second timescale. Both conformational states bound a CRIPT peptide with similar affinities but with different rates, and the distribution of the two conformational states was slightly shifted upon CRIPT binding. Our results are consistent with recent structural findings of conformational changes in PSD-95 and demonstrate how conformational transitions in supertertiary structures can shape the ligand-binding energy landscape and modulate protein–protein interactions.

Detailed characterization of protein-mediated interactions is a critical task for understanding cellular processes as well as for identification of novel drug targets. From an experimental perspective, a quantitative description of protein-mediated networks demands detection of specific interactions, followed by an attempt to understand larger systems. It should be noted, however, that describing protein interaction networks is a daunting task complicated by several factors that could be hard to estimate within the cellular environment, such as concentrations of individual proteins and compartmentalization. Additionally, proteins may experience conformational changes that may be difficult to capture but nevertheless modulate their function. Thus, a combination of structural, functional, and computational approaches is generally necessary to understand the role of conformational changes.

Postsynaptic density protein-95 (PSD-95) is a multidomain protein abundant in the postsynaptic density of neurons, where it acts as a scaffolding protein (1). Starting from the N terminus, this protein contains three PDZ domains followed by an Src homology 3 (SH3)[3] domain and a guanylate kinase-like (GK) domain (2). The PDZ domain is one of the most common protein interaction domains in our proteome (3). It presents a binding groove on its surface in which protein ligands can bind as a β-strand to form an extended β-sheet with the PDZ domain. PSD-95 contains a supertertiary structure (4); the first two PDZ domains form one supramodule (5), whereas the third PDZ domain (PDZ3) forms another supramodule together with the SH3 and GK domains (denoted PSG) (6–9) (Fig. 1). This feature is shared by other membrane-associated GK family proteins (10), to which PSD-95 belongs. In general, PDZ domains display similar affinity for a range of protein ligands (11) so that specificity must rely on spatial and temporal control in the cell. Because of this, it is often difficult to pinpoint natural ligands of PDZ domains, but a likely native ligand of PDZ3 from PSD-95 and of PDZ3 from its closely related paralog SAP97 is CXXC repeat– containing interactor of PDZ3 domain (CRIPT) (12, 13). PDZ3 binds the C terminus of CRIPT with a K_d of around 0.3 μM, and this affinity is achieved mainly via interactions between the six C-terminal residues of CRIPT (YKQTSV) and the binding groove of PDZ3 (14–16). However, several recent studies have highlighted the role of context dependence and more or less well-defined interactions outside of the binding motif for modular protein–protein interactions (17–20), mechanisms for which conformational transitions are likely important.

In this study, we investigated the binding kinetics of the PSG supramodule from human PSD-95 with a CRIPT peptide and

This work was funded in part by the European Union's Horizon 2020 Research and Innovation Program under Marie Sklodowska-Curie Grant Agreement 675341 (to S. G. and P. J.) and by Swedish Research Council Grant 2016-04965 (to P. J.). The authors declare that they have no conflicts of interest with the contents of this article.

[1] To whom correspondence may be addressed. E-mail: Stefano.Gianni@uniroma1.it.

[2] To whom correspondence may be addressed. E-mail: Per.Jemth@imbim.uu.se.

[3] The abbreviations used are: SH, Src homology; GK, guanylate kinase-like; CRIPT, CXXC repeat–containing interactor of PDZ3 domain; ITC, isothermal titration calorimetry; DJ, double jump.

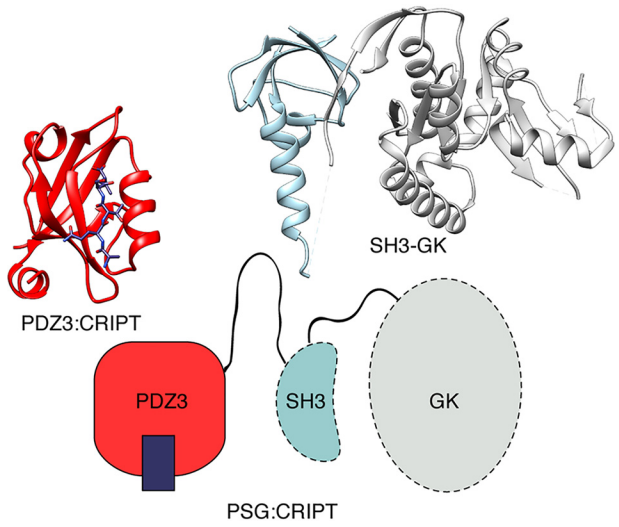

Figure 1. Structure of the PSG supramodule from PSD-95. Schematic supertertiary structure of the PSG supramodule from PSD-95 together with crystal structures of PDZ3 with a bound CRIPT peptide (PDB code 1BE9) and of the SH3-GK tandem (PDB code 1JXO).

found that the simplest mechanistic model consistent with the data involves two distinct conformational states of PSG. The two interconverting states can both bind a short CRIPT peptide with a similar affinity, but only one of the states can bind a longer CRIPT peptide. Moreover, the rate constants differ so that one conformer binds CRIPT faster than the other one, reflecting changes around the binding groove associated with the conformational transition. Previous work demonstrated conformational transitions within the PSG using structural approaches (8, 9), and more recently, functional oligomerization has been shown to be dependent on the PSG supramodule (17, 21–23). The binding kinetics observed in this study could be related to these phenomena.

Results

The binding kinetics of PSG and a six-amino-acid CRIPT peptide displayed biphasic behavior

We monitored binding of CRIPT to PSG using an N-terminal dansyl group attached to the six C-terminal residues of CRIPT (*D*-CRIPT$_6$). The dansyl quenches the fluorescence of an engineered Trp in PSG. The Trp was situated in the same position in PDZ3 (residue 337) as in previous studies of the isolated PDZ3 domain, where it did not affect affinity or kinetics of binding (16). Quenching of the Trp upon binding resulted in kinetic traces with high signal to noise (Fig. 2*A*). We previously performed extensive experiments with isolated PDZ3 and *D*-CRIPT$_6$ that yielded single exponential traces as pseudo-first-order conditions were approached, consistent with an apparent two-state binding mechanism (16, 24). However, fitting of the kinetic binding data of the PSG supramodule and *D*-CRIPT$_6$ to a single exponential function consistently yielded residuals displaying a clear nonrandom distribution around zero, even at *D*-CRIPT$_6$ concentrations 10-fold higher than those of PSG (Fig. 2), suggesting a more complex mechanism than two-state. A double-exponential equation fitted well to the experimental traces recorded over 1 s, and the observed rate constants, k_{obs1} and k_{obs2}, obtained from the fit were determined over a range of *D*-CRIPT$_6$ concentrations (Fig. 2*C*). The apparently linear dependence of both rate constants on *D*-CRIPT$_6$ concentration suggests that the PSG sample contained two distinct species, both of which could bind *D*-CRIPT$_6$, one with an association rate constant, k_{on1}, of $5.8 \times 10^6\ M^{-1}\ s^{-1}$ (from k_{obs1}) and the other with a k_{on2} of $\sim 0.56 \times 10^6\ M^{-1}\ s^{-1}$ (from k_{obs2}). In terms of amplitudes of the kinetic traces, k_{obs1} had a relatively large and k_{obs2} a relatively small amplitude (Fig. 2*D*). The k_{off} values could not be determined directly from these binding data because they were too low to allow accurate extrapolation of k_{obs} to zero *D*-CRIPT$_6$ concentration.

Displacement experiments corroborated the presence of two distinct molecular species

To investigate the dissociation kinetics of the PSG:CRIPT complex, we performed displacement experiments in which a preformed complex of PSG:*D*-CRIPT$_6$ (1 and 5 μM final concentrations) was rapidly mixed with an excess (100–200 μM) of unlabeled CRIPT peptide. In contrast to what we observed previously for the isolated PDZ3 domain (16, 24), the dissociation kinetics of PSG:*D*-CRIPT$_6$ were also biphasic (Fig. 3*A*), which strongly supports the presence of two distinct binding-competent PSG conformers. In fact, in a displacement experiment, any sequential mechanism, such as induced fit, usually yield kinetic dissociation transients that are well-described by single-exponential kinetics. The observed rate constants, which approximate the overall apparent dissociation rate constants (k_{off}^{app}), were approximately $k_{off1}^{app} = 1.35\ s^{-1}$ and $k_{off2}^{app} = 0.17\ s^{-1}$, respectively (Fig. 3*B*). The errors in the amplitudes were large because of covariation of the parameters, a common phenomenon in curve fitting of complex models (25). Nevertheless, based on six independent experiments, we found that the fast phase (described by k_{off1}^{app}) was associated with a relatively smaller amplitude and the slow phase (described by k_{off2}^{app}) with a relatively higher amplitude (Fig. 3*C*).

Affinity between PSG and CRIPT, determined by isothermal titration calorimetry, confirmed an affinity in the low micromolar range

From the kinetic data, it is not clear which k_{off}^{app} belongs to which k_{on}. We therefore performed ITC experiments to obtain an independent estimate of K_d. ITC experiments at the temperature of the stopped flow (10 °C) resulted in poor thermograms, but experiments at 20 °C, 25 °C, 30 °C, and 35 °C yielded good data (Fig. 4). The K_d values at 20 °C–30 °C were all around 0.2 μM, and we deem it likely that the affinity is similar at 10 °C. The two K_d values obtained from the ratios of rate constants, k_{off1}^{app}/k_{on1} (0.23 μM) and k_{off2}^{app}/k_{on2} (0.30 μM), respectively, are in very good agreement with the ITC data. This K_d is also close to that obtained for the isolated PDZ3 domain (15, 16). On the other hand k_{off1}^{app}/k_{on2} and k_{off2}^{app}/k_{on1} would give K_d values of 29 nM and 2.4 μM, respectively. Thus, the equilibrium binding data were most consistent with a scenario where k_{off1}^{app} and k_{on1} are associated with the binding to one conformer (denoted PSG_A) and k_{off2}^{app} and k_{on2} to the other conformer (PSG_B).

However, a model with two noninterconverting conformers predicts that the larger association amplitude should be con-

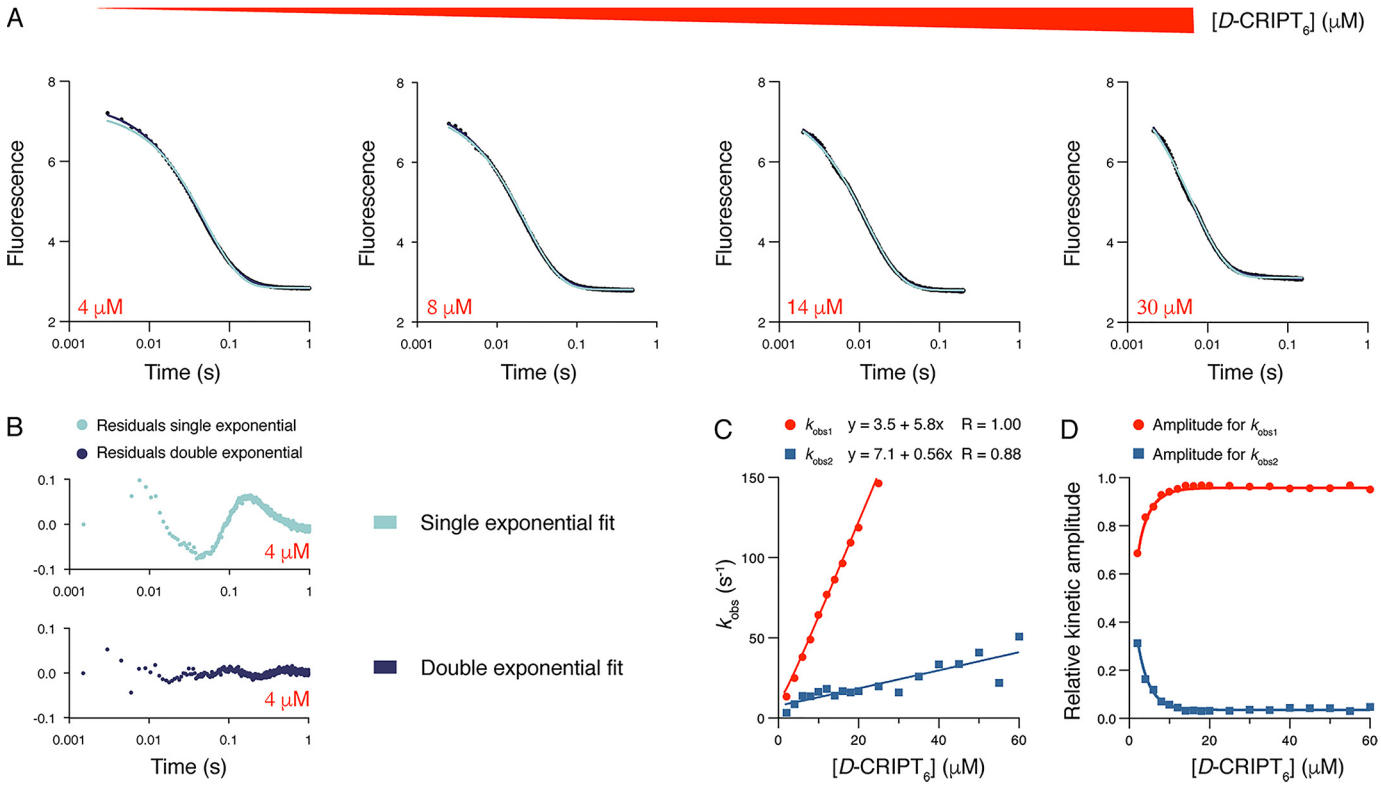

Figure 2. Binding kinetics of the PSG supramodule and CRIPT. *A*, example of kinetic transients for the association of PSG with *D*-CRIPT$_6$. PSG (1 μM final concentration) was mixed rapidly in the stopped flow with *D*-CRIPT$_6$ at different concentrations. *B*, the residuals are from fits to single- and double-exponential functions, respectively, at 4 μM final concentration of *D*-CRIPT$_6$. *C*, the experiment was repeated over a range of *D*-CRIPT$_6$ concentrations, and the k_{obs} values obtained from the fit to a double-exponential function were plotted *versus* [*D*-CRIPT$_6$]. k_{obs} values of more than 150 s^{-1} were omitted because they very slightly but progressively deviated from a straight line because of instrumental limitations in the mixing. *D*, kinetic amplitudes associated with the respective k_{obs} value.

nected to the larger dissociation amplitude. This is inconsistent with the relative amplitudes of the observed kinetic phases. Although the large variation in dissociation amplitudes precludes a detailed quantitative analysis, it is qualitatively clear that the kinetic amplitude of k_{off2}^{app} (Fig. 3*C*) is more prominent than that associated with k_{obs2} in the binding experiment (Fig. 2*D*). The most likely explanation for this discrepancy is that there is an equilibrium between PSG_A and PSG_B and that this equilibrium is shifted so that relatively more PSG_B is present upon binding of *D*-CRIPT$_6$ (Fig. 5).

Direct detection of the conformational transition in a double-jump interrupted binding experiment

In an attempt to directly monitor a transition between PSG_A and PSG_B in their bound conformation according to the scheme in Fig. 5, we performed interrupted binding experiments in a double-jump setup in the stopped flow instrument (Fig. 6*A*). 2 μM PSG was mixed with 4 μM *D*-CRIPT$_6$ in the "first jump" (concentrations after 1:1 mixing). After a defined delay (or aging) ranging between 10 ms and 200 s, this complex was dissociated by mixing with a large excess of unlabeled CRIPT in the "second jump." Following this second jump, the apparently irreversible dissociation kinetics of PSG:*D*-CRIPT$_6$ were monitored as described for a regular dissociation experiment, which, in practice, corresponds to an interrupted binding experiment with a very long delay time. We collected 14 kinetic traces from these double-jump experiments, with delay times between 10 ms and 200 s. The trace at 10 ms delay time was excluded because the mismatch between expected and actual delay time was deemed too large. Next, all remaining dissociation traces (delay times between 24 ms and 200 s) were fitted simultaneously to a double-exponential function with shared values for k_{off1}^{app} and k_{off2}^{app}, either locked to the average values reported in Fig. 3*B* or free-fitted (Fig. 6*B*). This is possible because the final conditions under which kinetics were measured were identical for each double-jump experiment. However, it is also necessary to perform a simultaneous fit because the kinetic amplitudes at short delay times are too small for accurate free-fitting of k_{off1}^{app} and k_{off2}^{app}. Next, the kinetic amplitudes associated with k_{off1}^{app} and k_{off2}^{app} were plotted as a function of delay time (Fig. 6, *C* and *D*). The change in the kinetic amplitudes over time followed biphasic behavior, as clearly seen for the amplitude related to k_{off1}^{app}. This biphasic behavior reflects the initial build-up of the two complexes, PSG_A:*D*-CRIPT$_6$ and PSG_B:*D*-CRIPT$_6$, respectively, followed by their equilibration. The change in the amplitudes over time thus follows exponential kinetics. We could fit a double-exponential function to the amplitude data and obtain two observed rate constants. However, the errors were very large, and this experiment is best interpreted qualitatively or semiquantitatively; k_{obs1}^{DJ} (DJ, double jump) was around 20–40 s^{-1} and k_{obs2}^{DJ} in the range of 0.1–0.8 s^{-1}, depending on which set of amplitudes was used. Thus, at short delay times, both amplitudes increased with increasing delay time with an apparent rate constant, which corresponds to the binding of *D*-CRIPT$_6$

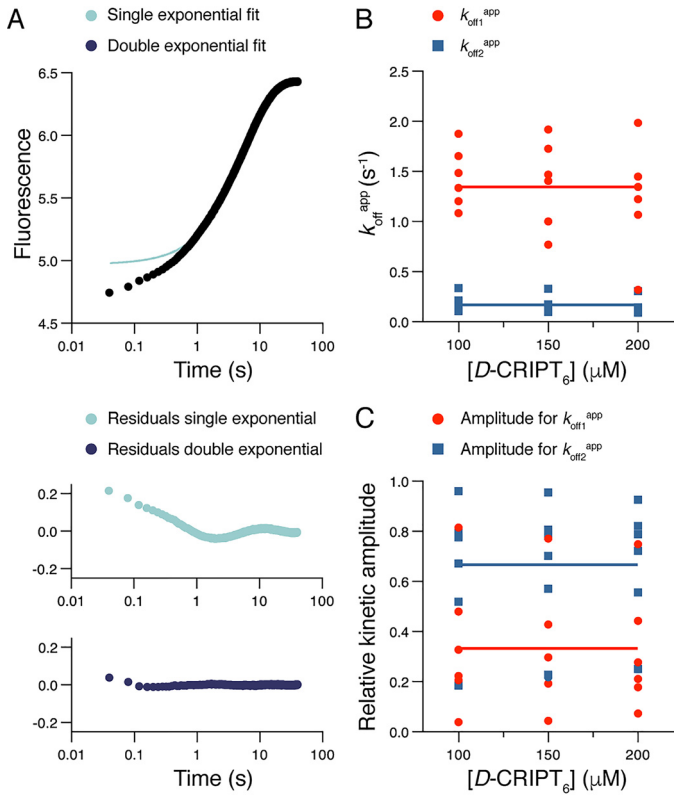

Figure 3. Dissociation kinetics of the PSG supramodule and *D*-CRIPT$_6$. *A*, example of kinetic trace from an experiment where a complex of PSG and *D*-CRIPT$_6$ (2 and 10 μM) was rapidly mixed with an excess of unlabeled CRIPT (150 μM). The resulting trace was fitted to a single or double exponential, and the residuals from the respective fit are presented below the trace. The double-exponential fit yielded the following parameters: k_{off1}^{app} = 1.35 s^{-1} (amplitude = 0.32) and k_{off2}^{app} = 0.16 s^{-1} (amplitude = 1.4). *B* and *C*, this experiment was repeated six times, each time at three different concentrations of unlabeled CRIPT (100, 150, and 200 μM). The double-exponential fit yielded k_{off}^{app} values (*B*) and their associated amplitudes (*C*, normalized), which were plotted *versus* CRIPT concentration. The large scatter in the points, in particular for the amplitudes, reflects the covariation of parameters in the curve fitting. The average of all 18 k_{off}^{app} values for each kinetic phase yielded the following parameters: k_{off1}^{app} = 1.35 ± 0.42 s^{-1} and k_{off2}^{app} = 0.17 ± 0.08 s^{-1} (indicated by *horizontal lines* in *B*). The average of all 18 amplitudes yielded the following values: Amp_1 = 0.33 ± 0.24 and Amp_2 = 0.67 ± 0.24 (indicated by *horizontal lines* in *C*).

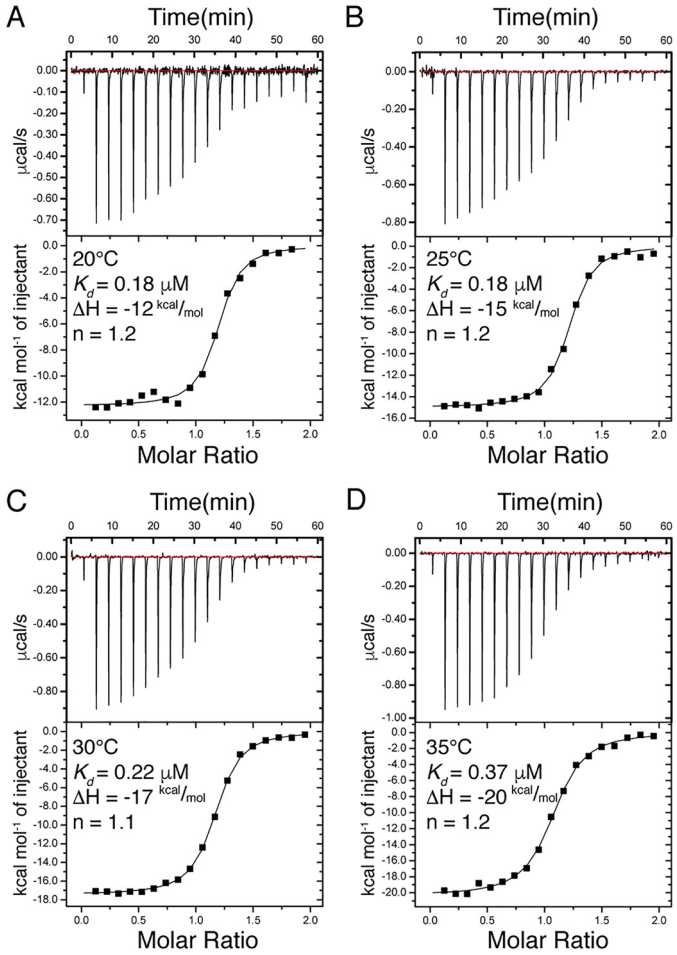

Figure 4. Isothermal titration calorimetry experiments with PSG and *D*-CRIPT$_6$. *A–D*, ITC experiments were performed at four different temperatures (20 °C–35 °C). The parameters shown were obtained by fitting a 1:1 binding model using the software provided with the instrument. The K_d values from these experiments agreed well with those calculated from the kinetic experiments at 10 °C (k_{off1}^{app}/k_{on1} or k_{off2}^{app}/k_{on2}).

to PSG and which, at least for k_{obs1}^{DJ}, is in excellent agreement with the parameters obtained from single-jump binding experiments ($k_{obs1}^{DJ} \approx k_{on1} \times 4\ \mu M + k_{off1}^{app} \approx 25\ s^{-1}$). At longer delay times, the kinetic phase associated with k_{off1}^{app} decreases, whereas the phase associated with k_{off2}^{app} should increase (the latter is not as clear as the former because of scatter in the data). This reflects the redistribution of conformations in the bound complex occurring over 1–10 s with a net flow from PSG$_A$:*D*-CRIPT$_6$ to PSG$_B$:*D*-CRIPT$_6$ (Fig. 5).

Global fitting of a minimal model for the interaction between PSG and D-CRIPT$_6$

To test the robustness of the kinetic scheme in Fig. 5, we attempted a global fit of kinetic transients from binding and dissociation experiments using the Kintek software (26, 27). Global fitting with numerical integration takes information from both rate constants and kinetic amplitudes into consideration. The information from kinetic amplitudes is often overlooked but can, in favorable cases, be used to distinguish between kinetic models. However, in the case of fluorescence-monitored measurements, this requires knowledge about the fluorescence yields of all molecular species, and those of intermediates are usually unknown. Here, the information from the kinetic amplitudes was used to restrain the parameters in the model. Thus, a global fit of a dataset, including seven binding curves from Fig. 2*C* and all dissociation curves from the double-jump experiment (Fig. 6), was performed, and it resulted in reasonable kinetic parameters (Fig. 7).

A comparison of the globally fitted rate constants with those obtained from fitting binding and dissociation transients individually shows that, although k_{on1} is similar, k_{on2} from the global fit is 4-fold larger than in Fig. 2*C*. The main reason is that we could not include the data points at high concentrations of *D*-CRIPT$_6$ in the global curve fitting because the binding step described by k_{on1} and k_{off1}^{app} gets too fast. It is clear that k_{on2} is closer to 0.6 $\mu M^{-1}\ s^{-1}$ (Fig. 2*C*) than to 2.2 $\mu M^{-1}\ s^{-1}$ obtained from the global fit. k_{off1} and k_{off2} are also more similar to each other in the global fit than k_{off1}^{app} and k_{off2}^{app} in the individual fits presented in Fig. 3. However, the values of k_{off1} and k_{off2} in the global fit are dependent on the relative values of k_3 and k_{-3}, which are poorly defined. The rate constants k_{-3} and k_3 agree

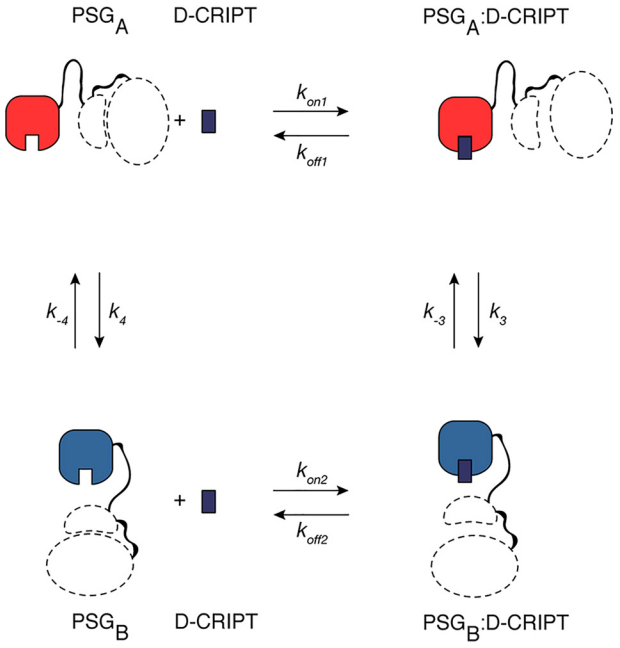

Figure 5. A kinetic scheme consistent with the binding kinetics of PSG and *D*-CRIPT$_6$. A scenario with two conformations, PSG$_A$ and PSG$_B$, which are in equilibrium and can both bind CRIPT, is consistent with the kinetic and equilibrium data. Access to the binding groove is more restricted in the PSG$_B$ conformation.

well with the fit of the double-jump data in Fig. 6 insofar as their sum is 0.53 s^{-1}. Finally, k_{-4} and k_4 are fitted as 0.007–0.018 s^{-1}, but they are obviously very poorly defined, except that this step must be relatively slow relative to the other ones. In summary, despite low accuracy for several of the fitted rate constants, global fitting (Fig. 7) shows that the experimental data are overall consistent with the proposed minimal model depicted in Fig. 5 for the interaction between PSG and *D*-CRIPT$_6$.

Binding kinetics of a 15-mer CRIPT peptide are monophasic

To further investigate the conformational transition in the PSG supramodule, we performed binding experiments with an *N*-dansylated peptide corresponding to the 15 C-terminal residues of CRIPT, *D*-CRIPT$_{15}$. In contrast to *D*-CRIPT$_6$, we only observed single exponential kinetics with *D*-CRIPT$_{15}$ in both binding and displacement experiments (Fig. 8). The apparent rate constants (k_{on} and k_{off}) for *D*-CRIPT$_{15}$ were more similar to k_{on1} and k_{off1}^{app}, associated with the fast phase for *D*-CRIPT$_6$, and giving a similar K_d (0.42 μM) as *D*-CRIPT$_6$. The K_d determined by ITC for *D*-CRIPT$_{15}$ was 1.6 $\pm$ 0.2 μM at a higher temperature (25 °C), in fair agreement with K_d from kinetics. One explanation, considering the close match of the k_{on} values, would be that *D*-CRIPT$_{15}$ can only bind to PSG$_A$ but not to PSG$_B$. However, even with *D*-CRIPT$_6$, the kinetic amplitude of the slow phase is low, and for the longer *D*-CRIPT$_{15}$ it may not be visible. Regardless of whether *D*-CRIPT$_{15}$ binds to PSG$_B$, this conformation is present in equilibrium with PSG$_A$, as monitored by the smaller *D*-CRIPT$_6$, which can likely access a more narrow binding pocket present in PSG$_B$.

Discussion

Much of our current knowledge regarding protein-mediated interactions is based on study of isolated domains in solution. Nevertheless, it is clear that, because proteins are dynamic entities, the interaction between contiguous domains may play a role in their structure and function. A hallmark of these interactions is represented by hemoglobin, a system where it was established how the intricate interplay between the four subunits results in very complex binding schemes that ultimately mediate allosteric regulation and fine-tune oxygen (un)binding to optimize its transport from the lungs to tissues. Although the dynamics of allosteric multisubunit proteins have a long history (28), recent work has been focused on multidomain proteins in which several distinct protein domains occur in one single polypeptide as beads on a string. It is becoming clear that such proteins often display supertertiary structures (4) where supramodules could form from two or several domains, which may then cooperate positively or negatively in ligand binding or other functions. Similarly to hemoglobin, simplified models must be used to account for the behavior of such multidomain proteins.

The MAGUK family of proteins, to which PSD-95 belongs, is one class of multidomain proteins that has been well-studied, in particular from the point of view of single domains but also from the perspective of its two supramodules. We previously determined binding rate constants for the isolated PDZ3 domain and established that its interaction with CRIPT is a one-step process (16, 24). Here we extended these studies to the PSG supramodule, which consists of PDZ3 and two more domains, SH3 and GK, and found that a model with two conformations, denoted PSG$_A$ and PSG$_B$, can satisfactorily describe the data. Although PSG$_A$ binds CRIPT with similar rate constants as PDZ3, PSG$_B$ appears to display a more restricted binding pocket.

Previous work on PSG from the PSD-95 family or other homologs has not assessed the mechanism with direct kinetic methods. However, multiple complementary methods, including crystallography, NMR, small-angle X-ray scattering, single-molecule FRET, binding experiments, and modeling, have demonstrated that the three domains form a well-defined and dynamic supertertiary structure (8–10, 29, 30). For example, single-molecule FRET in PSD-95 showed that PDZ3 displays motional averaging relative to the SH3 domain (8). Furthermore, NMR, small-angle X-ray scattering, and simulations were consistent with distinct structural ensembles in free PSG and CRIPT-bound PSG, where the ensemble of bound conformations was shifted toward extended rather than compact species (9). In more detail, the peptide-binding groove of PDZ3 has been shown to interact weakly with the SH3 domain (or the linker between them) so that, in the ligand-free state, the SH3 domain restricts ligand binding to PDZ3. Binding of a ligand to PDZ3 would thus promote a more open conformation of PSG where SH3 is released from PDZ3. These conformational transitions could be the basis of the biphasic kinetics observed in this study. From a functional perspective, PSD-95 forms oligomers in the postsynaptic density, and one way is via the SH3 and GK domains (6). This oligomerization is mediated by ligand binding to PDZ3 (21). Furthermore, ligand binding to PDZ3 promotes binding of GK to other proteins, such as the G protein subunit Gnb5 (23) but restricts binding of another protein, GukHolder (29). These previous studies are consistent with our

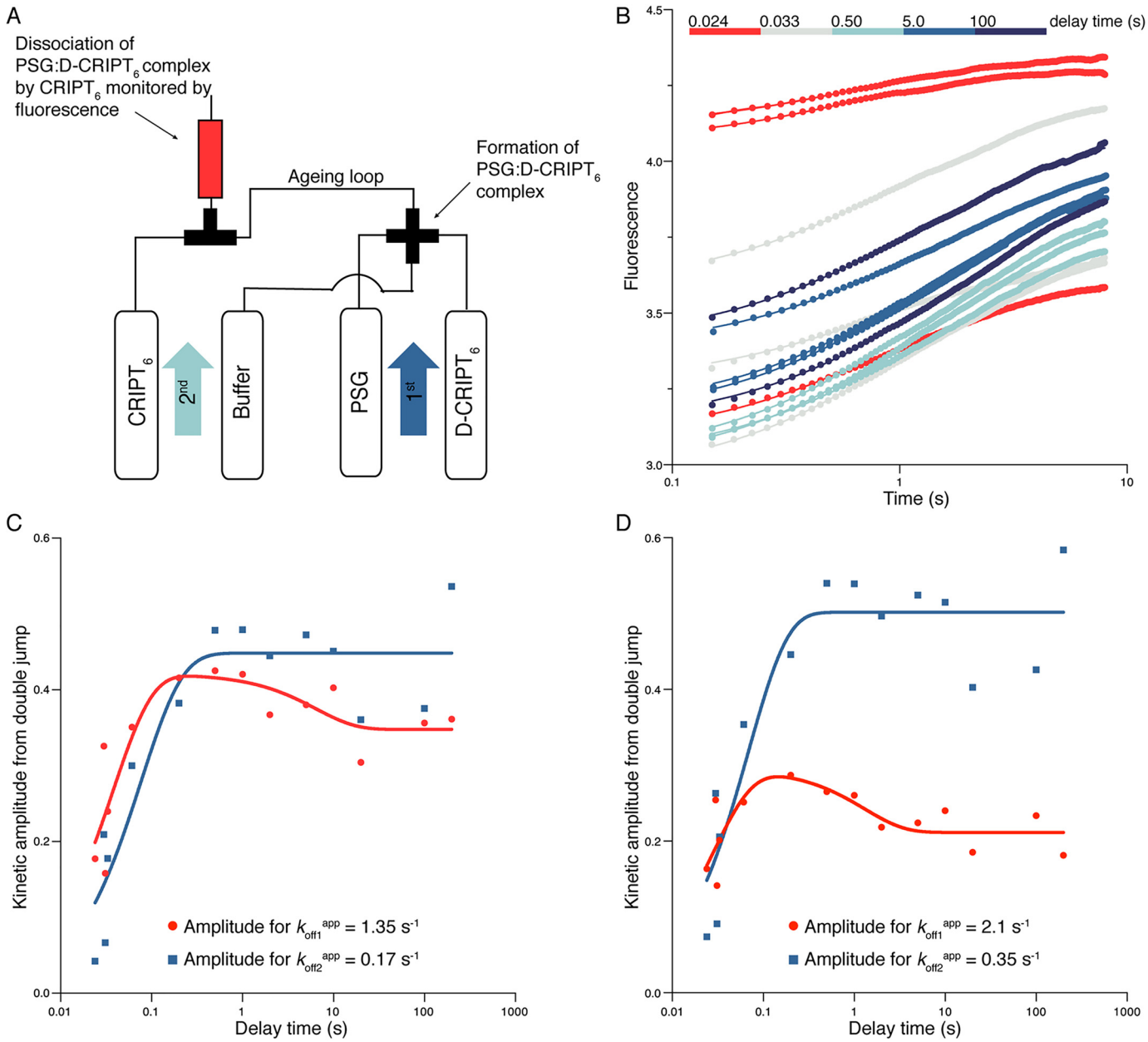

Figure 6. Interrupted binding experiments. *A*, schematic of the double-jump setup. In the first jump, 4 μM PSG was mixed with 8 μM *D*-CRIPT$_6$ (*i.e.* the final concentrations after mixing were 2 μM and 4 μM, respectively) and incubated for a certain delay time in an aging loop. Following the set delay time, any formed complex was dissociated by a large excess of unlabeled CRIPT in a second jump (final concentrations were 1 μM PSG, 2 μM *D*-CRIPT$_6$, and 50 μM unlabeled CRIPT). *B*, the dissociation kinetics were monitored in the flow cell. The kinetic traces were fitted simultaneously to a double-exponential function with either locked k_{obs} values (the two average k_{off}^{app} values from single-jump experiments, 1.35 s^{-1} and 0.17 s^{-1}, respectively) or shared and free-fitted k_{obs} values (k_{off1}^{app} = 2.1 s^{-1} and k_{off2}^{app} = 0.35 s^{-1}). The best fit curves in the figure correspond to the latter fit. *C* and *D*, the kinetic amplitudes from the respective fits in *B* were plotted against delay time. This reflects the build up of PSG$_A$:*D*-CRIPT$_6$ and PSG$_B$:*D*-CRIPT$_6$, respectively, with time. These amplitude data, in turn, were fitted to a double-exponential function to obtain two "observed double-jump rate constants" for the build up of PSG$_A$ and PSG$_B$, respectively. From the fit, k_{obs}^{DJ} values of around 20–40 s^{-1} and 0.1–0.8 s^{-1}, respectively, were obtained. Although the parameters are underdetermined, it is clear that there is an initial increase in the respective population, followed by a decrease in PSG$_A$:*D*-CRIPT$_6$. The expected concomitant increase in PSG$_B$:*D*-CRIPT$_6$ is lost in the experimental noise.

kinetic data insofar as the binding kinetics suggest that the PSG$_B$ conformation is less accessible than PSG$_A$, as mirrored by the differences in k_{on1} (PSG$_A$) and k_{on2} (PSG$_B$) upon binding to *D*-CRIPT$_6$, and that *D*-CRIPT$_{15}$ apparently only binds to PSG$_A$. A more restricted binding site provides fewer possibilities of productive initial encounters, reducing the apparent association rate constant. It is possible that the more open PSG$_A$ is the conformation allowing SH3-GK-mediated oligomerization and binding between GK and the G protein subunit Gnb5 (17, 21–23).

In conclusion, there is a firm structural basis for a dynamic supertertiary structure of the PSG from PSD-95 (8, 9). This dynamic behavior is characterized by some distinctive kinetic signatures, as highlighted by our kinetic analysis. Furthermore, our experiments estimate a timescale of these transitions of about 0.5 s^{-1} at 10 °C. We speculate that such conformational

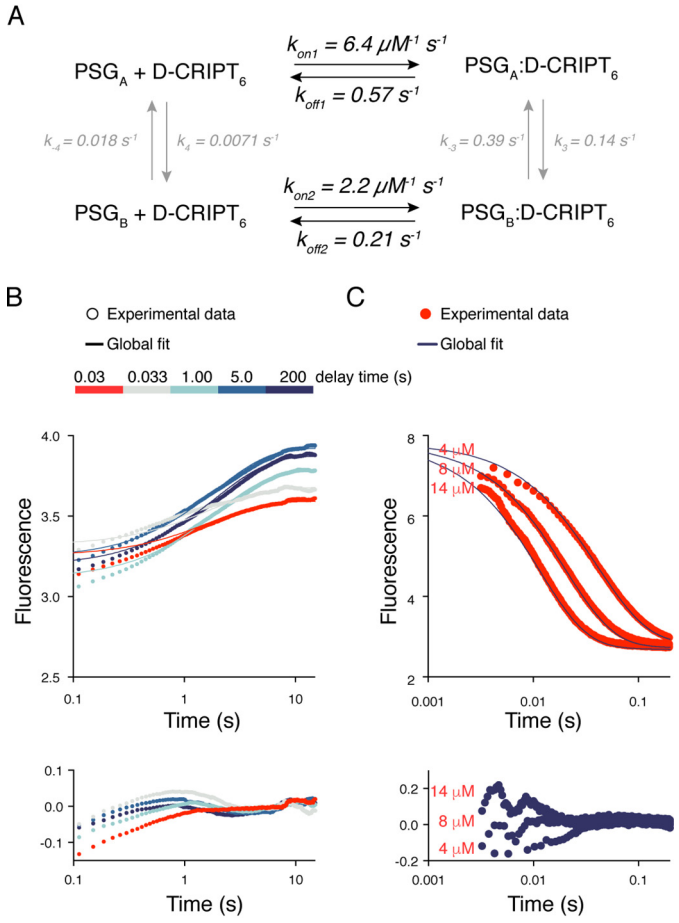

Figure 7. Global fitting to a minimal scheme describing PSG:CRIPT binding. Data from binding and dissociation kinetic experiments were fitted globally with KinTek Explorer. *A*, the scheme shows the fitted square model with the best fit parameters and their standard errors. The amplitude factors for PSG$_A$:*D*-CRIPT$_6$ and PSG$_B$:*D*-CRIPT$_6$ were fitted to 0.9 ± 0.1 and 0.13 ± 0.03, respectively. It should be noted that the reported standard errors for all parameters are likely underestimated. We used the global fit to qualitatively test our suggested minimal model. Thus, less emphasis should be put on the estimates of the microscopic rate constants, which are, in some cases, poorly constrained. k_{on2} is likely overestimated because we could only use lower *D*-CRIPT$_6$ concentrations in the global fit to capture the fast phase (Fig. 2). *B*, fit of interrupted binding stopped flow data to the minimal model in *A*. Five kinetic traces are shown for clarity. The residuals of the fits are shown below the curve. *C*, fit of the single-jump stopped-flow data to the model, with residuals shown below the curves. The fits to kinetic traces of three different concentrations of *D*-CRIPT$_6$ are shown for clarity.

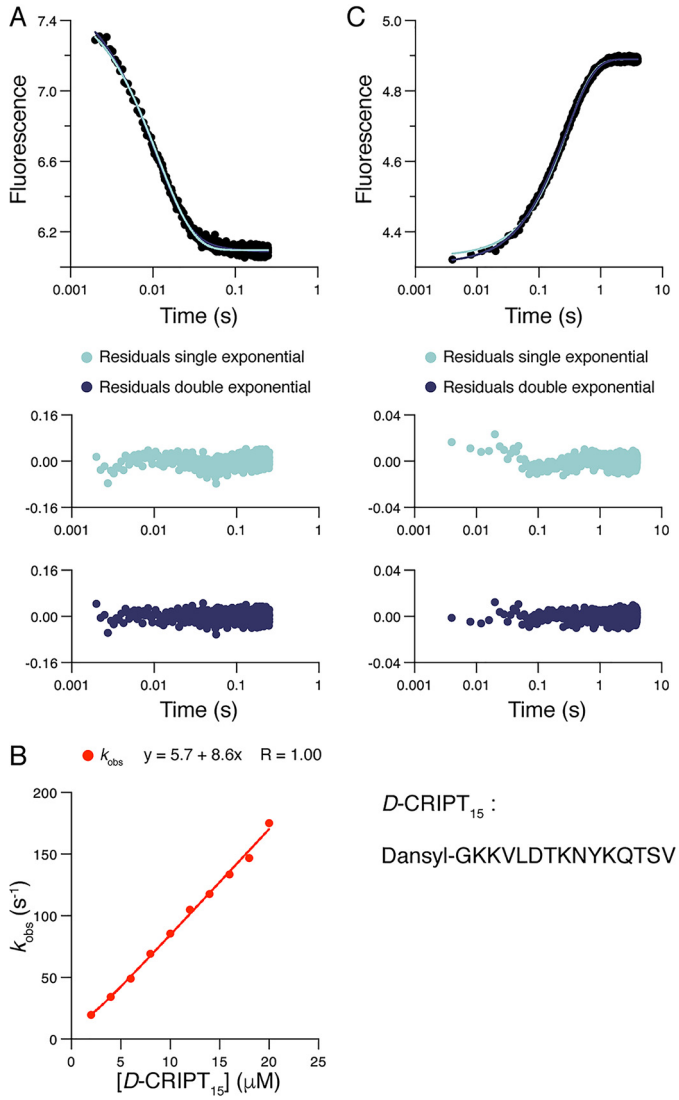

Figure 8. Binding kinetics of the PSG supramodule and *D*-CRIPT$_{15}$. *A*, PSG (1 μM final concentration) was mixed rapidly in the stopped flow with *D*-CRIPT$_{15}$ (10 μM final concentration). A single-exponential function well describes the experimental transient, as shown by comparison of residuals from fit to single- and double-exponential functions. *B*, the experiment was repeated over a range of *D*-CRIPT$_{15}$ concentrations, and k_{obs} obtained from the fit to a single-exponential function was plotted *versus* [*D*-CRIPT$_{15}$] to obtain k_{on}^{app} = (8.4 ± 0.2) × 10^6 M^{-1} s^{-1} (fitting error). *C*, dissociation of the complex. PSG:*D*-CRIPT$_{15}$ (2 and 10 μM) was rapidly mixed with an excess of unlabeled CRIPT (150 μM). The resulting trace was fitted to both single- and double-exponential functions. The residuals from the fits show that the dissociation kinetics follow single exponential kinetics. The average of three experiments using 100, 150, and 200 μM CRIPT, respectively, for displacement yielded k_{off}^{app} = 3.5 ± 0.011 s^{-1} (± S.D.).

transitions in the PSG are related to the previously reported conformational changes and are most likely connected to its function, as demonstrated previously in several studies (17, 21–23, 29). Future work based on site-directed variants will further explore the functional role of these transitions.

Experimental procedures

Protein purification

The PSD-95 PDZ3-SH3-GK (PSG) supramodule (residues 308–724) contained an engineered Trp in the same position (F337W) as in previous studies of the isolated PDZ3 domain (16, 24). PSG was expressed from a modified pRSET plasmid (Invitrogen), which was transformed into *Escherichia coli* BL21(DE3) pLys cells. The cells were grown in lysogeny broth (LB) medium at 37 °C until A_{600} of the culture reached 0.6. Then overexpression of protein was induced with 1 mM isopropyl β-D-thiogalactopyranoside, and the bottles were incubated overnight in a rotary shaker at 18 °C. Cells were harvested by centrifugation at 4 °C, and the pellet was resuspended in 50 mM Tris (pH 7.8), 100 mM NaCl, and 10% glycerol and stored at −20 °C until purification. The pellet was thawed and sonicated twice for 4 min each time, followed by centrifugation. The supernatant was filtered and loaded onto a nickel-Sepharose Fast Flow column (GE Healthcare) pre-equilibrated with 50 mM Tris, 100 mM NaCl, 10% glycerol, and 0.5 mM DTT. The column was washed with equilibration buffer, and bound protein was

eluted with 250 mM imidazole. The protein sample was dialyzed overnight into 50 mM Tris, 2 mM DTT, 100 mM NaCl, and 10% glycerol. The PSG sample was concentrated and further purified using size exclusion chromatography (S-100, GE Healthcare). Protein purity was quantified by SDS-PAGE and identity by MALDI-TOF MS. Concentrations of protein samples were measured by absorbance at 280 nm and theoretical extinction coefficients based on the amino acid composition. Far-UV CD spectra (200–260 nm) of the protein (10 μM) were recorded to ensure that it was folded. CD experiments were performed in 50 mM sodium phosphate (pH 7.45) and 21 mM KCl (I = 150) at 10 °C on a JASCO J-1500 spectropolarimeter using the average of five scans.

Kinetic methods

All kinetic experiments were performed in 50 mM sodium phosphate (pH 7.45), 21 mM KCl (I = 150 mM), 0.5 mM tris(2-carboxyethyl)phosphine at 10 °C. Kinetic binding and dissociation experiments were performed in an upgraded SX-17 MV stopped-flow spectrophotometer (Applied Photophysics, Leatherhead, UK) and carried out as described previously (16). Briefly, k_{on} was obtained from binding experiments approaching pseudo-first-order conditions ([PSG] < [*D*-CRIPT]). PSG (1 μM) was rapidly mixed with different concentrations of N-terminally dansyl-labeled CRIPT. The shorter peptide, dansyl-YKQTSV, was denoted *D*-CRIPT$_6$, and the longer one, dansyl-GKKVLDTKNYKQTSV, was denoted *D*-CRIPT$_{15}$. The binding reaction was monitored by fluorescence, where the Trp at position 337 in PDZ3 was quenched by the dansyl group of the CRIPT peptide. Trp 337 was excited at 280 nm, and emission was followed at 330 nm (using a 330 ± 25 nm interference filter). Kinetic traces were recorded and averaged (a minimum of five individual traces were used at each concentration) and fitted to single- or double-exponential functions to obtain the k_{obs} for each CRIPT concentration. To estimate k_{on} values, k_{obs1} and k_{obs2} (for PSG with *D*-CRIPT$_6$) or k_{obs} (for PSG with *D*-CRIPT$_{15}$) were plotted *versus* CRIPT concentration and fitted to a linear function, where the slope corresponds to k_{on}. Because of slow dissociation rates, k_{off} could not be accurately determined by extrapolation of k_{obs} to zero CRIPT in the binding experiments. Thus, displacement experiments were performed to obtain more accurate estimates of k_{off}. In these experiments, PSG (2 μM) was preincubated with *D*-CRIPT$_6$ (10 μM). *D*-CRIPT$_6$ was then displaced from PSG by rapidly mixing the complex with an excess of unlabeled CRIPT$_6$ (100, 150, and 200 μM). The high excess of unlabeled peptide ensured an irreversible dissociation reaction, allowing k_{off} to be estimated from the average of three experiments in which k_{obs} ($\approx k_{off}$) did not change with CRIPT$_6$ concentration. Similar to binding, all displacement experiments performed with PSG and *D*-CRIPT$_6$ were fitted to a double-exponential function, yielding two distinct observed dissociation rate constants.

Double-jump mixing experiments were performed on an Applied Photophysics SX18-MV stopped-flow instrument according to the manufacturer's instructions with regard to mixing volumes. In particular, a solution containing 4 μM PSG in the presence of 50 mM phosphate buffer (pH 7.5) was first mixed 1:1 with *D*-CRIPT$_6$ peptide at an initial concentration of 8 μM. Then, after a controlled delay time (between 10 ms and 200 s), the solution was challenged with a high concentration of unlabeled CRIPT$_6$ in a second mixing event (the initial concentration of CRIPT$_6$ was 100 μM. Thus, the final concentrations in the displacement reaction were 1 μM PSG, 2 μM *D*-CRIPT$_6$, and 50 μM unlabeled CRIPT. In analogy to single-mix stopped-flow experiments, the double-jump experiment was carried out at 10 °C and analyzed as described under "Results."

Global fitting of kinetic data

Kinetic transients from single- and double-jump stopped-flow experiments were fitted globally to a minimal model (Fig. 5) using KinTek Explorer (26, 27). This software utilizes numerical integration and allows fitting of raw kinetic data directly to a mechanistic model. The interrupted binding experiments, with delay times varying from 24 ms to 200 s, were included in the global fit together with binding experiments in which [*D*-CRIPT$_6$] varied between 2–14 μM. For practical reasons, the lower boundary of k_4 and k_{-4} was set to 10^{-5} s^{-1} in the fitting procedure. k_{on} for the CRIPT$_6$ peptide used in dissociation experiments (with no dansyl group) was locked to be the same as for *D*-CRIPT$_6$, and k_{off} was locked to 0 (irreversible binding is practically achieved at concentrations where CRIPT$_6$ ≫ *D*-CRIPT$_6$). The remaining parameters in the model were fitted without constrains. To account for baseline shifts in the double-jump kinetic experiments, constants were added to the output expressions. A scaling factor was used to account for the difference in total fluorescence output between the single-jump and double-jump stopped-flow experiments.

Isothermal titration calorimetry

Isothermal titration calorimetry (ITC) experiments were performed in 50 mM sodium phosphate (pH 7.45), 21 mM KCl (I = 150), and 0.5 mM tris(2-carboxyethyl)phosphine at 20 °C, 25 °C, 30 °C, and 35 °C in an iTC200 instrument (Malvern). *D*-CRIPT$_6$ and PSG were dialyzed overnight in the same buffer to minimize artifacts from buffer mismatch. *D*-CRIPT$_6$ (220 μM) was titrated (16–19 injections) into a cell containing 22 μM PSG, and saturation was obtained by having approximately a two times excess of *D*-CRIPT$_6$. Baseline correction was performed manually to minimize the χ value in the curve fitting using the software provided with the iTC200 instrument.

Author contributions—L. L. data curation; L. L., E. K., S. G., and P. J. formal analysis; L. L. and E. K. investigation; L. L. and E. K. visualization; L. L., E. K., and S. G. methodology; L. L., E. K., S. G., and P. J. writing-review and editing; S. G. and P. J. conceptualization; P. J. resources; P. J. supervision; S. G. and P. J. funding acquisition; P. J. writing-original draft; P. J. project administration.

References

1. Sheng, M., and Kim, E. (2011) The postsynaptic organization of synapses. *Cold Spring Harb. Perspect. Biol.* **3,** pii: a005678 CrossRef Medline
2. Feng, W., and Zhang, M. (2009) Organization and dynamics of PDZ-domain-related supramodules in the postsynaptic density. *Nat. Rev. Neurosci.* **10,** 87–99 CrossRef Medline

3. Ivarsson, Y. (2012) Plasticity of PDZ domains in ligand recognition and signaling. *FEBS Lett.* **586,** 2638–2647 CrossRef Medline
4. Tompa, P. (2012) On the supertertiary structure of proteins. *Nat. Chem. Biol.* **8,** 597–600 CrossRef Medline
5. Long, J.-F., Tochio, H., Wang, P., Fan, J.-S., Sala, C., Niethammer, M., Sheng, M., and Zhang, M. (2003) Supramodular structure and synergistic target binding of the N-terminal tandem PDZ domains of PSD-95. *J. Mol. Biol.* **327,** 203–214 CrossRef Medline
6. McGee, A. W., Dakoji, S. R., Olsen, O., Bredt, D. S., Lim, W. A., and Prehoda, K. E. (2001) Structure of the SH3-guanylate kinase module from PSD-95 suggests a mechanism for regulated assembly of MAGUK scaffolding proteins. *Mol. Cell.* **8,** 1291–1301 CrossRef Medline
7. Tavares, G. A., Panepucci, E. H., and Brunger, A. T. (2001) Structural characterization of the intramolecular interaction between the SH3 and guanylate kinase domains of PSD-95. *Mol. Cell.* **8,** 1313–1325 CrossRef Medline
8. McCann, J. J., Zheng, L., Rohrbeck, D., Felekyan, S., Kühnemuth, R., Sutton, R. B., Seidel, C. A., and Bowen, M. E. (2012) Supertertiary structure of the synaptic MAGuK scaffold proteins is conserved. *Proc. Natl. Acad. Sci.* **109,** 15775–15780 CrossRef Medline
9. Zhang, J., Lewis, S. M., Kuhlman, B., and Lee, A. L. (2013) Supertertiary structure of the MAGUK core from PSD-95. *Structure* **21,** 402–413 CrossRef Medline
10. Pan, L., Chen, J., Yu, J., Yu, H., and Zhang, M. (2011) The structure of the PDZ3-SH3-GuK tandem of ZO-1 protein suggests a supramodular organization of the membrane-associated guanylate kinase (MAGUK) family scaffold protein core. *J. Biol. Chem.* **286,** 40069–40074 CrossRef Medline
11. Tonikian, R., Zhang, Y., Sazinsky, S. L., Currell, B., Yeh, J.-H., Reva, B., Held, H. A., Appleton, B. A., Evangelista, M., Wu, Y., Xin, X., Chan, A. C., Seshagiri, S., Lasky, L. A., Sander, C., *et al.* (2008) A specificity map for the PDZ domain family. *PLoS Biol.* **6,** e239 CrossRef Medline
12. Niethammer, M., Valtschanoff, J. G., Kapoor, T. M., Allison, D. W., Weinberg, R. J., Craig, A. M., and Sheng, M. (1998) CRIPT, a novel postsynaptic protein that binds to the third PDZ domain of PSD-95/SAP90. *Neuron* **20,** 693–707 CrossRef Medline
13. Zhang, L., Jablonski, A. M., Mojsilovic-Petrovic, J., Ding, H., Seeholzer, S., Newton, I. P., Nathke, I., Neve, R., Zhai, J., Shang, Y., Zhang, M., and Kalb, R. G. (2017) SAP97 binding partner CRIPT promotes dendrite growth *in vitro* and *in vivo*. *eNeuro* **4,** pii: ENEURO.0175–17.2017 CrossRef Medline
14. Doyle, D. A., Lee, A., Lewis, J., Kim, E., Sheng, M., and MacKinnon, R. (1996) Crystal structures of a complexed and peptide-free membrane protein-binding domain: molecular basis of peptide recognition by PDZ. *Cell* **85,** 1067–1076 CrossRef Medline
15. Saro, D., Li, T., Rupasinghe, C., Paredes, A., Caspers, N., and Spaller, M. R. (2007) A thermodynamic ligand binding study of the third PDZ domain (PDZ3) from the mammalian neuronal protein PSD-95. *Biochemistry* **46,** 6340–6352 CrossRef Medline
16. Gianni, S., Haq, S. R., Montemiglio, L. C., Jürgens, M. C., Engström, Å., Chi, C. N., Brunori, M., and Jemth, P. (2011) Sequence-specific long range networks in PSD-95/discs large/ZO-1 (PDZ) domains tune their binding selectivity. *J. Biol. Chem.* **286,** 27167–27175 CrossRef Medline
17. Zeng, M., Ye, F., Xu, J., and Zhang, M. (2018) PDZ ligand binding-induced conformational coupling of the PDZ-SH3-GK tandems in PSD-95 family MAGUKs. *J. Mol. Biol.* **430,** 69–86 CrossRef Medline
18. Pascoe, H. G., Gutowski, S., Chen, H., Brautigam, C. A., Chen, Z., Sternweis, P. C., and Zhang, X. (2015) Secondary PDZ domain-binding site on class B plexins enhances the affinity for PDZ-RhoGEF. *Proc. Natl. Acad. Sci. U.S.A.* **112,** 14852–14857 CrossRef Medline
19. Ivarsson, Y., and Jemth, P. (2019) Affinity and specificity of motif-based protein-protein interactions. *Curr. Opin. Struct. Biol.* **54,** 26–33 Medline
20. Erlendsson, S., Thorsen, T. S., Vauquelin, G., Ammendrup-Johnsen, I., Wirth, V., Martinez, K. L., Teilum, K., Gether, U., and Madsen, K. L. (2019) Mechanisms of PDZ domain scaffold assembly illuminated by use of supported cell membrane sheets. *eLife* **8,** e39180 Medline
21. Rademacher, N., Kunde, S.-A., Kalscheuer, V. M., and Shoichet, S. A. (2013) Synaptic MAGUK multimer formation is mediated by PDZ domains and promoted by ligand binding. *Chem. Biol.* **20,** 1044–1054 CrossRef Medline
22. Zeng, M., Shang, Y., Araki, Y., Guo, T., Huganir, R. L., and Zhang, M. (2016) Phase transition in postsynaptic densities underlies formation of synaptic complexes and synaptic plasticity. *Cell* **166,** 1163–1175.e12 CrossRef Medline
23. Rademacher, N., Kuropka, B., Kunde, S.-A., Wahl, M. C., Freund, C., and Shoichet, S. A. (2019) Intramolecular domain dynamics regulate synaptic MAGUK protein interactions. *eLife* **8,** e41299 Medline
24. Gianni, S., Engström, A., Larsson, M., Calosci, N., Malatesta, F., Eklund, L., Ngang, C. C., Travaglini-Allocatelli, C., and Jemth, P. (2005) The kinetics of PDZ domain-ligand interactions and implications for the binding mechanism. *J. Biol. Chem.* **280,** 34805–34812 CrossRef Medline
25. Bagshaw, C. R. (2017) *Biomolecular kinetics: A Step-by-Step Guide*, CRC Press, Boca Raton, FL
26. Johnson, K. A., Simpson, Z. B., and Blom, T. (2009) Global kinetic explorer: a new computer program for dynamic simulation and fitting of kinetic data. *Anal. Biochem.* **387,** 20–29 CrossRef Medline
27. Johnson, K. A., Simpson, Z. B., and Blom, T. (2009) FitSpace explorer: an algorithm to evaluate multidimensional parameter space in fitting kinetic data. *Anal. Biochem.* **387,** 30–41 CrossRef Medline
28. Monod, J., Wyman, J., and Changeux, J. P. (1965) On the nature of allosteric transitions: a plausible model. *J. Mol. Biol.* **12,** 88–118 CrossRef Medline
29. Qian, Y., and Prehoda, K. E. (2006) Interdomain interactions in the tumor suppressor discs large regulate binding to the synaptic protein GukHolder. *J. Biol. Chem.* **281,** 35757–35763 CrossRef Medline
30. Nomme, J., Fanning, A. S., Caffrey, M., Lye, M. F., Anderson, J. M., and Lavie, A. (2011) The Src homology 3 domain is required for junctional adhesion molecule binding to the third PDZ domain of the scaffolding protein ZO-1. *J. Biol. Chem.* **286,** 43352–43360 CrossRef Medline